Inorganic Chemistry

ARTICLE

pubs.acs.org/IC

Three-Step Calcination Synthesis of High-Purity Li_8ZrO_6 with CO_2 Absorption Properties

Xian-Sheng Yin, Qin-Hui Zhang,* and Jian-Guo Yu

State Key Lab of Chemical Engineering, College of Chemical Engineering, East China University of Science and Technology, Shanghai 200237, People's Republic of China

Supporting Information

ABSTRACT: Li_8ZrO_6 contains a high lithium content and may bear a great ability of CO_2 absorption, yet the reports about the properties of CO_2 absorption on Li_8ZrO_6 are few to date for its difficulty in production. In this paper, high-purity Li_8ZrO_6 is synthesized via a three-step calcination method combined with an effective lithium source and a suitable initial Li/Zr molar ratio. The produced Li_8ZrO_6 possesses a great CO_2 absorption capacity of about 53.98 wt % at 998 K, which could be well-maintained in a wide range of CO_2 partial pressures of 0.1−1.0 bar although it decreased gradually during the multicycle process of CO_2 absorption−desorption in a 10% CO_2 feed stream because of the high working temperature. These properties imply that Li_8ZrO_6 may be a new option for high-temperature CO_2 capture applied in industrial processes such as a steam methane reformer.

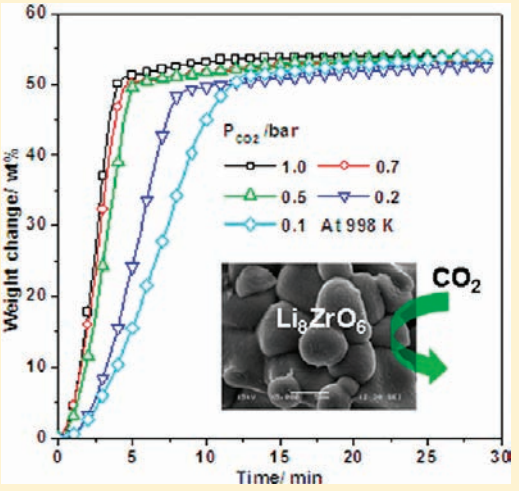

INTRODUCTION

CO_2 separation is important in the industrial processes such as hydrocarbon reforming and purification, and CO_2 capture from the flue gas of coal-burning power plants is also one of the possible solutions to eliminating the amount of CO_2 emitted to the atmosphere.[1−3] The CO_2 produced in the above processes is generally hot and coexisted with other typical gases of H_2, CO, N_2, and H_2O.[4,5] In view of the energy efficiency, it is more advisible to capture CO_2 at high temperature directly without cooling the gas stream to ambient temperature prior to CO_2 removal,[6,7] yet the key problem is the suitable CO_2 absorbent with high stability and capacity at high temperature. Various materials have been proposed and developed as CO_2 absorbents,[8−14] in which lithium-based ceramics present good properties as CO_2 absorbents for high capacity and selectivity at 773−1013 K.[14] Li_2ZrO_3 was first reported as a CO_2 absorbent by Nakagawa and Ohashi[15] in 1998 and considered to be a promising candidate of CO_2 capture; after Li_2ZrO_3, several other lithium-based ceramics such as Li_4SiO_4,[16,17] $Li_6Zr_2O_7$,[18,19] and Li_5AlO_4[20] were also reported as high-temperature CO_2 absorbents. However, the CO_2 concentration in the industrial processes is normally low (10−13%), and the CO_2 absorption capacity for most of the reported lithium-based ceramics is strongly limited by the partial pressure of CO_2 (P_{CO_2}) in the feed stream.[4,5,16,19] Thereby, it is highly desired to find a new absorbent with an effective capacity of CO_2 absorption in a low CO_2 concentration atmosphere.

Li_8ZrO_6 is well-known as a tritium breeder material with advantages in safety, a lack of electromagnetic effects, and tritium release.[21−23] It was also reported that Li_8ZrO_6 shows a high ionic conductivity and could be used as a conduction material.[24] However, reports about the properties of CO_2 absorption on Li_8ZrO_6 are few to date despite the likely great CO_2 absorption capacity for its high lithium content.[14] One of the reasons is the difficulty in the synthesis of pure Li_8ZrO_6. Wyers and Cordfunke[22] synthesized Li_8ZrO_6 under vacuum with ZrO_2 and Li_2O obtained by thermal decomposition of LiOH; Zou and Petric[23] prepared Li_8ZrO_6 using ZrO_2 and Li_2O_2 through complicated heat-treating procedures. The reported synthesis methods of pure Li_8ZrO_6 were not convenient and were difficult to repeat under common experimental conditions. In this study, pure Li_8ZrO_6 is synthesized via a simple three-step calcination process, and the properties of CO_2 absorption including the effect of temperature, influence of the CO_2 concentration, and multicycle stability are investigated systematically.

Received: October 7, 2010
Published: February 28, 2011

EXPERIMENTAL METHODS

Experimental Procedures. Zirconium nitrate [$Zr(NO_3)_4 \cdot 5H_2O$] and lithium nitrate ($LiNO_3$) were used as precursors (Shanghai Chemical Co., Shanghai, China). Appropriate amounts of each reagent were dissolved in deionized water and mixed with vigorous stirring; after volatilization of the solvent at 363 K, the achieved powder was grounded and reacted via a three-step calcination process in the muffle. At the first step (calcination at 873 K for 2 h), $Zr(NO_3)_4$ was decomposed as amorphous ZrO_2 and dispersed in the molten $LiNO_3$; then, to avoid spilling over the crucible, the calcination temperature was enhanced to 1073 K for another 2 h to convert the molten $LiNO_3$ as solid-state Li_2O and reacted with ZrO_2 to produce $Li_6Zr_2O_7$ particles, which was further reacted with excessive Li_2O to produce a Li_8ZrO_6 layer on the particle surface. Finally, the calcination temperature was enhanced to 1173 K for 72 h to improve diffusion of Li_2O through the external Li_8ZrO_6 layer and convert the internal $Li_6Zr_2O_7$ as Li_8ZrO_6 completely. Additionally, lithium hydroxide ($LiOH \cdot H_2O$; Shanghai Chemical Co., Shanghai, China) was chosen as a lithium resource to compare the influence of different lithium sources for the synthesis of pure Li_8ZrO_6.

Characterization of the Samples. The crystalline structures were characterized by X-ray diffraction (XRD; Rigaku, D/max-RB using Cu Kα Ni-filtered radiation with $\lambda = 1.5406$ Å), scanning in the 2θ range of 10−80° with a 10° min^{-1} step size. The relative percentages of different crystal phases presented in the products were estimated semiquantitatively from the total areas under the most intense diffraction peak of each phase identified.[25,26] The morphology of the products was analyzed by a scanning electron microscope (JSM-6360 LV), and the samples were pretreated by covering with gold to overcome their lack of electron conductivity. The Brunauer−Emmett−Teller (BET) specific surface area was determined by a N_2 adsorption−desorption method at a liquid-nitrogen temperature (77 K) using a Micromeritics ASAP-2010C instrument, and the samples were pretreated at 523 K for 3 h in a vacuum.

The CO_2 uptake properties were tested under defined conditions using a thermogravimetric analyzer (SDTQ600), and the testing processes were similar to those in our previous report:[19] For each test, about 15 mg samples were installed in the sample pan and heated from room temperature to the working temperature with 20 K min^{-1} in a N_2 atmosphere. Then the N_2 flow was switched to the testing gas, and the CO_2 absorption process was started. The regenerability test was conducted by heating the CO_2 absorbed sample in a N_2 flow at appropriate temperatures. The multicycle test was conducted under the conditions of uptake in a 10% CO_2 atmosphere and desorption in a N_2 atmosphere at suitable temperatures for enough time, respectively.

RESULTS AND DISCUSSION

Synthesis and Characterization of Pure Li_8ZrO_6. Figure 1 shows the XRD analysis of the achieved products prepared using $LiNO_3$ and $Zr(NO_3)_4$. Patterns a−d correspond to the samples of Li/Zr molar ratios at 8.0, 10.0, 12.0, and 14.0, respectively; pattern e is the standard pattern of rhombohedral-phase Li_8ZrO_6 (JCPDS 26-0867, $a = 5.48$ Å, and $c = 15.45$ Å). As can be seen, the diffraction peaks of pattern a are comprised of monoclinic-phase $Li_6Zr_2O_7$ (JCPDS 34-0312, $a = 10.45$ Å, $b = 5.99$ Å, and $c = 10.21$ Å) and rhombohedral-phase Li_8ZrO_6, and the peaks of $Li_6Zr_2O_7$ are weakened in patterns b and c when the Li/Zr molar ratio is increased to 14.0; the corresponding pattern d is comprised of only rhombohedral-phase Li_8ZrO_6. Figure 2 presents the relationship between the initial Li/Zr molar ratios and the content of Li_8ZrO_6 in the products. Because the initial Li/Zr molar ratio is 8.0, the percentage of Li_8ZrO_6 in product a is only about 43.79%,

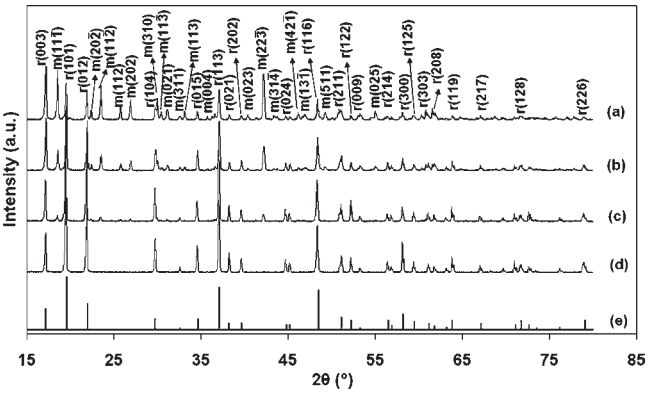

Figure 1. XRD pattern of samples synthesized by calcination at 1173 K using $LiNO_3$ and $Zr(NO_3)_4$. Patterns a−d correspond to the sample prepared with Li/Zr molar ratios at 8.0, 10.0, 12.0, and 14.0, respectively. Pattern e corresponds to the standard pattern of rhombohedral-phase Li_8ZrO_6. m(*hkl*): monoclinic-phase $Li_6Zr_2O_7$. r(*hkl*): rhombohedral-phase Li_8ZrO_6.

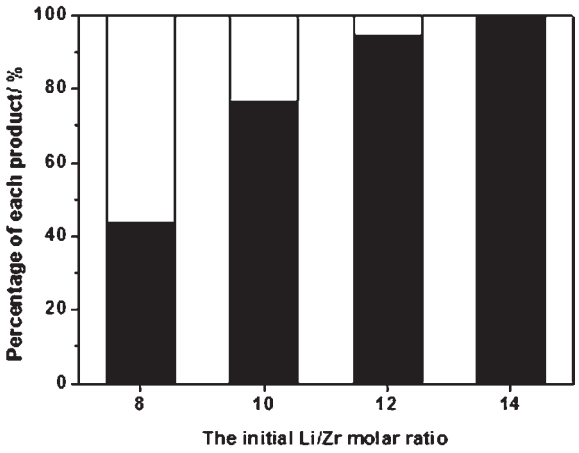

Figure 2. Percentages for $Li_6Zr_2O_7$ and Li_8ZrO_6 in the products synthesized as a function of the initial Li/Zr molar ratio. □: monoclinic-phase $Li_6Zr_2O_7$. ■: rhombohedral-phase Li_8ZrO_6.

further increasing the initial Li/Zr molar ratios to 10.0, 12.0, and 14, and the percentage of Li_8ZrO_6 in each of the achieved products is 76.39%, 94.34%, and 100%, respectively. This result indicates that sublimation of Li_2O decomposed from $LiNO_3$ is very serious during the recrystallization process, and the production of pure Li_8ZrO_6 needs about 75% surplus lithium source in the initial Li/Zr molar ratios. On the basis of the above analysis, the synthesis mechanism of Li_8ZrO_6 could be speculated as eqs 1 and 2.

$$3Li_2O + 2ZrO_2 \rightarrow Li_6Zr_2O_7 \quad (1)$$

$$Li_6Zr_2O_7 + 5Li_2O \rightarrow 2Li_8ZrO_6 \quad (2)$$

The choice of $LiNO_3$ as the lithium source is another crucial factor in the synthesis of Li_8ZrO_6. When lithium hydroxide ($LiOH \cdot H_2O$) is used instead of $LiNO_3$, the $Li_6Zr_2O_7$ impurity is always presented in the products, even increasing the initial Li/Zr molar ratio up to 20.0 (see Figures S1 and S2 in the Supporting Information). Analysis of the scanning electron microscopy (SEM) reveals that the products synthesized using

dx.doi.org/10.1021/ic102035y |*Inorg. Chem.* 2011, 50, 2844–2850

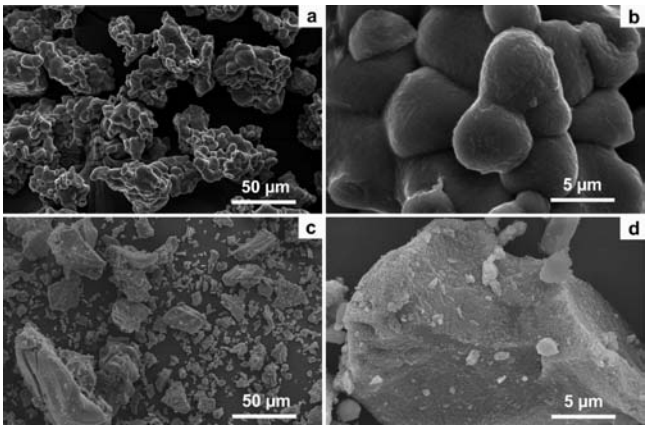

Figure 3. SEM images of samples synthesized using different lithium sources with an initial Li/Zr molar ratio at 14.0. Images a and b correspond to the product of pure Li_8ZrO_6 synthesized using $LiNO_3$ and $Zr(NO_3)_4$. Images c and d correspond to the product synthesized using LiOH and $Zr(NO_3)_4$.

$LiNO_3$ and LiOH as lithium sources, respectively, exhibit very different morphologies. As can be seen in Figure 3, the product corresponding to $LiNO_3$ is build up by shapely particles with an average size of about 5.0 μm, indicating that an equable nucleation and growth process has happened, while the product corresponding to LiOH is composed of larger bulks with irregular shape, which may be due to the reaction (3) taking place in the process of solution mixture, and the produced $Zr(OH)_4$ may be further decomposed and sintered to ZrO_2 particles with very serious agglomeration during the heat treatment procedures; then $Li_6Zr_2O_7$ may be formed first with large particle sizes, resulting in limitation of the thermal diffusion of ions such as Li^+ and O^{2-}; subsequently, the internal $Li_6Zr_2O_7$ of the particle could not be further converted to Li_8ZrO_6 effectively.

$$4LiOH + Zr(NO_3)_4 \rightarrow Zr(OH)_4\downarrow + 4LiNO_3 \qquad (3)$$

Compared with the reported synthesis methods of Li_8ZrO_6, in which Li_2O (or Li_2O_2) and ZrO_2 were used as precursors and rigorous reaction conditions were required,[22−24] the proposed preparation method here presents several advantages: First, $LiNO_3$ is safer and more obtainable than Li_2O (or Li_2O_2); second, the designed three-step calcination process is effective in the formation of Li_8ZrO_6; third, the synthesis process is conducted under common conditions and can be repeated easily. These advantages represent significant improvements in the scope of Li_8ZrO_6 synthesis.

Kinetic Analysis of CO_2 Absorption and Desorption. Considering the varied concentrations of CO_2 produced in the industry procedures, the focus of this study is on the properties of CO_2 absorption on Li_8ZrO_6 in a series of mixed gases of CO_2 and N_2 with P_{CO_2} varied from 1.0 to 0.1 bar. Figure 4 presents the thermogravimetric behavior of sample Li_8ZrO_6 under an atmosphere of P_{CO_2} at 0.1 bar, which is close to the CO_2 concentration in the flue gas from a coal-burning power plant or the steam methane reformer (SMR) process. As can be seen, Li_8ZrO_6 has a very fast CO_2 absorption rate at temperatures up to 1000 K and starts to release CO_2 at temperatures higher than 1100 K, indicating that Li_8ZrO_6 is an effective high-temperature CO_2 captor with about 50 wt % capacity.

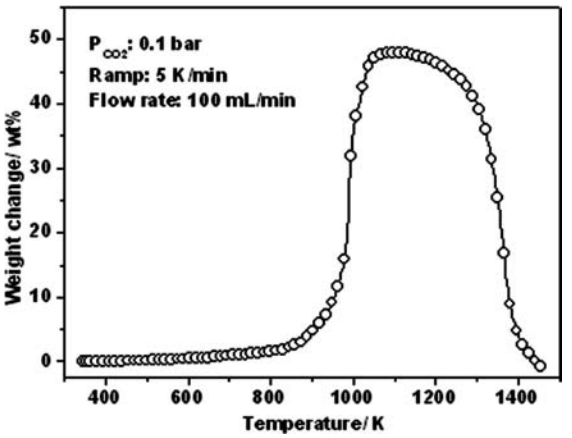

Figure 4. Thermogravimetric analysis curve of Li_8ZrO_6 analyzed in a flux of CO_2 with P_{CO_2} at 0.1 bar.

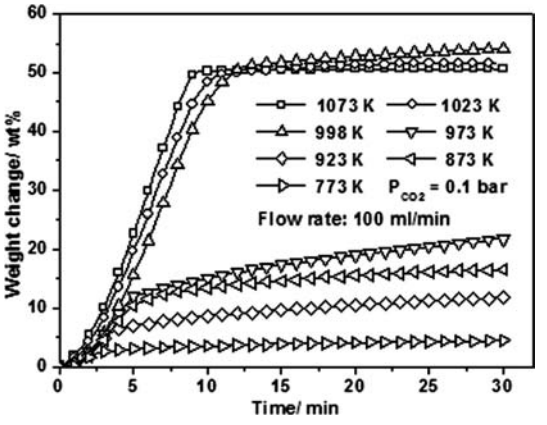

Figure 5. Kinetics of CO_2 absorption on Li_8ZrO_6 at different temperatures in a 10% CO_2 feed stream.

Further, the CO_2 absorption kinetics on Li_8ZrO_6 at various temperatures with P_{CO_2} at 0.1 bar are presented in Figure 5. At temperatures of 773−973 K, the CO_2 absorption rates are slow but increased gradually with enhancement of the operating temperature, suggesting that a solid-state carbonate shell might be formed on the surface of the particles during the CO_2 absorption process (the melting point of Li_2CO_3 was at about 983 K);[19] then at operating temperatures up to 998 K, a fast weight gain is taking place within the initial 10 min with a saturation capacity of 53.98 wt % weight gain; upon further enhancement of the temperature to 1023 and 1073 K, the CO_2 absorption rates are increased but not significantly, and the achieved capacities of CO_2 absorption are reduced fractionally compared with that at 998 K. The behaviors of CO_2 absorption on Li_8ZrO_6 at different temperatures are consistent with the results observed in Figure 4. The fast absorption behavior at 998 K may result from the facile diffusion of CO_2 in the molten carbonate shell and the improved thermal diffusion of ions (e.g., Li^+ and O^{2-}) in Li_8ZrO_6, and the fractional reduction of the CO_2 absorption capacities at 1023 and 1073 K may be attributed to the release of partially absorbed CO_2 at these temperatures.

The XRD patterns a−d shown in Figure 6 correspond to the CO_2-absorbed samples at 873, 923, 973, and 998 K for 30 min, respectively. As can be seen, some Li_2CO_3 (JCPDS 22-1141, a = 8.359 Å, b = 4.977 Å, and c = 6.194 Å) and $Li_6Zr_2O_7$ specific

dx.doi.org/10.1021/ic102035y |*Inorg. Chem.* 2011, 50, 2844–2850

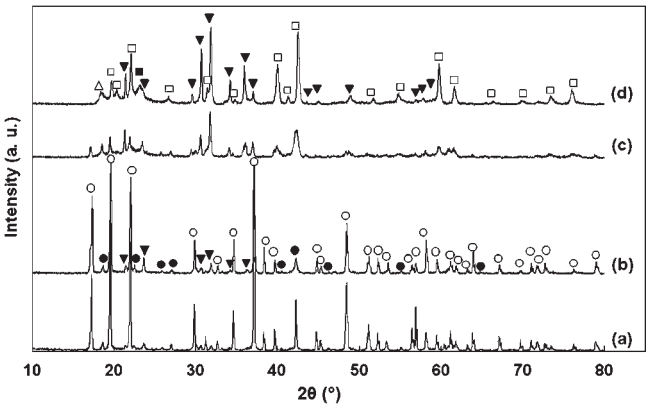

Figure 6. XRD analysis of the CO_2-absorbed Li_8ZrO_6 sample at 873, 923, 973, and 998 K corresponding to patterns a−d, respectively: ▼, Li_2CO_3; ■, Li_2ZrO_3 (JCPDS 20-0647); □, Li_2ZrO_3 (JCPDS 33-0843); ●, $Li_6Zr_2O_7$; Δ, unknown phase.

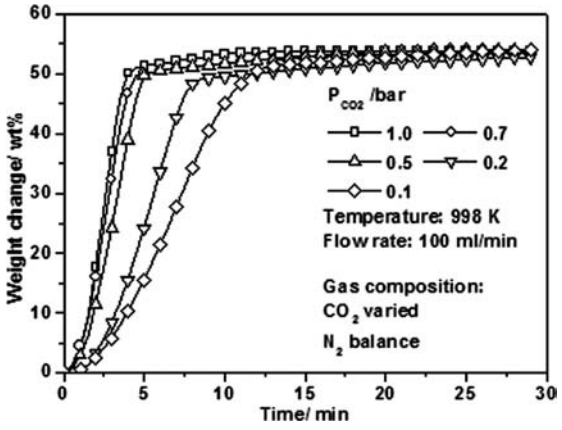

Figure 7. Curves of CO_2 absorption on Li_8ZrO_6 at 998 K as a function of the CO_2 concentration.

diffraction peaks appear in patterns a and b, and the diffraction peaks of $Li_6Zr_2O_7$ gradually disappear with enhancement of the absorption temperature. The CO_2-absorbed sample at 998 K is composed of Li_2ZrO_3 (JCPDS 33-0843, a = 5.427 Å, b = 9.031 Å, and c = 5.423 Å; JCPDS 20-0647, a = 9.0 Å, b = 9.0 Å, and c = 3.43 Å) and Li_2CO_3. Accordingly, the reaction mechanism during CO_2 absorption on Li_8ZrO_6 could be presented as eqs 4 and 5 with the theoretical CO_2 absorption capacity of 54.4 wt %, which is very close to the observed experimental results of 53.98 wt % (about 99.23% theoretical capacity) analyzed above.

$$Li_8ZrO_6 + CO_2 \rightarrow Li_6Zr_2O_7 + Li_2CO_3 \quad (4)$$

$$Li_6Zr_2O_7 + CO_2 \rightarrow 2Li_2ZrO_3 + Li_2CO_3 \quad (5)$$

Figure 7 shows the influence of P_{CO_2} on the absorption rate and the capacity of CO_2 absorption on Li_8ZrO_6 at 998 K. As P_{CO_2} was increased from 0.1 to 1.0 bar, the absorption rate increased from about 5.0 to 11.3 wt % min^{-1}, with the absorption capacities remaining almost invariable. This behavior is very different from that of the previously reported lithium-based ceramics such as Li_2ZrO_3, $Li_6Zr_2O_7$, and Li_4SiO_4. Figure 8 presents the variances of the absorption capacities as P_{CO_2} was decreased from 1.0 to 0.1 bar for the four kinds of lithium-based ceramics. The CO_2

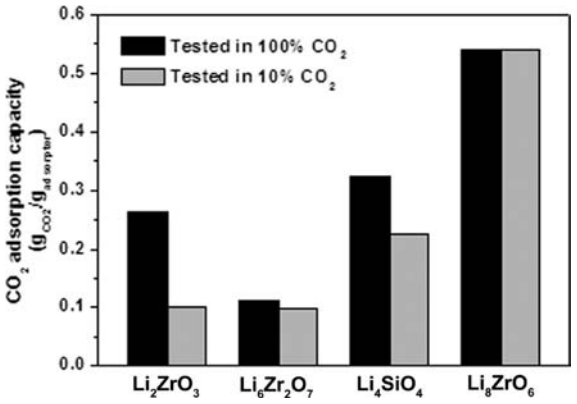

Figure 8. Comparison of CO_2 absorption capacities in pure CO_2 and 10% CO_2 atmospheres for different lithium-based ceramics.

absorption capacity for Li_2ZrO_3 was sharply reduced by about 80%,[4] and the losses of capacities for the higher lithium content materials of $Li_6Zr_2O_7$ and Li_4SiO_4 are lower but are still about 13.3% and 30.5%, respectively,[16,19] while Li_8ZrO_6 can preserve 100% capacity of CO_2 absorption, which is the highest capacity of CO_2 capture from the low CO_2 concentration atmosphere (10% volume content) for the lithium-based ceramics reported to date.[14] In fact, the capacities of CO_2 absorption for the lithium-based ceramics are closely related with the lithium content in the absorbents, and the absorbents with richer lithium content could offer more absorption sites in the absorption process.[14,19] Therefore, if the lithium content in the lithium-based ceramic is low, the rate of CO_2 absorption may be greatly slowed with a decrease of P_{CO_2} because of the reduction of the effective collision reaction, subsequently causing a loss of the achieved capacity of CO_2 absorption in the definite time; on the contrary, if the lithium content in the lithium-based ceramics is high enough, the amount of the effective collision reaction may be large even in the low CO_2 concentration atmosphere, and the capacity of CO_2 absorption may be maintained. These may be the main reasons for the different CO_2 absorption performances of the four kinds of lithium-based absorbents in the atmosphere of CO_2 concentrations in the range of 0.1−1.0 bar.

Generally, the product of Li_8ZrO_6 synthesized in this study represents significant improvements in the scope of high-temperature CO_2 absorption so far[14] and may be a new option for high-temperature CO_2 capture in industrial processes such as SMR (normally operated at 1073−1300 K).[3−5]

The regenerability of Li_8ZrO_6 after CO_2 absorption is also investigated by desorbing CO_2 at different temperatures in a N_2 flow of 250 mL min^{-1}. Figure 9 shows the CO_2 desorption curves of the CO_2-absorbed Li_8ZrO_6 sample (absorption at 998 K for 30 min in a 10% CO_2 atmosphere) regenerated at 1123, 1148, and 1173 K, respectively. As was expected previously, the absorbed CO_2 in Li_8ZrO_6 could be released under high temperatures; moreover, the regeneration rate is strongly dependent on the desorption temperature. At 1123 K, the desorption process is not complete even after 110 min; with an increase of the working temperature, the desorption rate is obviously sped up, and the absorbed CO_2 can be entirely released within about 80 and 50 min at 1148 and 1173 K, respectively.

Multicycle Performance of CO_2 Absorption−Desorption on Li_8ZrO_6. Further, Figure 10 shows the multicycle performance of CO_2 absorption−desorption on Li_8ZrO_6 under the conditions of absorption at 1023 K in a 10% CO_2 feed gas for

dx.doi.org/10.1021/ic102035y |*Inorg. Chem.* 2011, 50, 2844–2850

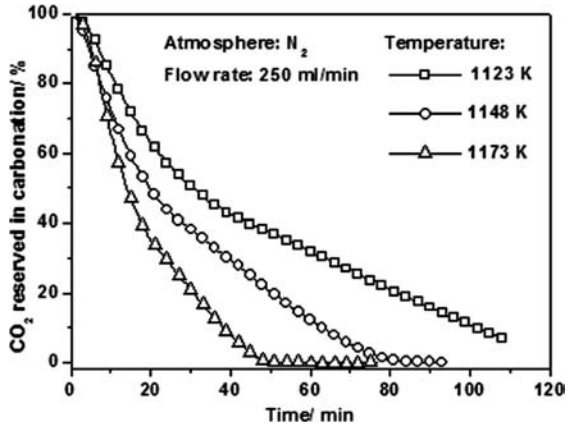

Figure 9. Kinetics of CO_2 desorption from the absorbed Li_8ZrO_6 at different temperatures in a N_2 atmosphere with a flow rate of 250 mL min^{-1}.

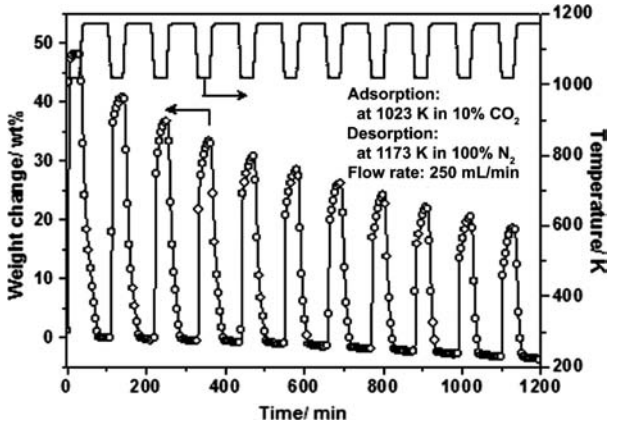

Figure 10. Multicycle performance of CO_2 absorption−desorption on Li_8ZrO_6 with the conditions of absorption at 1023 K in a 10% CO_2 feed stream and desorption at 1133 K in a N_2 flow with a flow rate of 250 mL min^{-1} via thermogravimetric analysis.

30 min and desorption at 1173 K in a N_2 flow for 65 min. With an increase of the cycle times, the absorption rate is decreased gradually and the achieved absorption capacity for the corresponding cycle is reduced subsequently; after 10 cycles, only about 45.01% capacity is preserved.

The reduced capacity during the multicycle process may be caused by the following two points. First, as can be seen in Figure 10, the fractional weight of the absorbent is lost during the multicycle process (about 3.08% weight is lost after 11 cycles) because of sublimation of Li_2O during the desorption processes under high temperature, which was also observed for $Li_6Zr_2O_7$ and Li_4SiO_4, and may result in the reduction of the CO_2 absorption capacity in the multicycle process.[14,19] However, the reduction of the capacity caused by the loss of Li_2O after 11 cycles is only about 6.24% by theoretical calculation, while the entire reduced capacity of the 11th cycle is about 54.99% compared with that of the 1st cycle. So, the loss of Li_2O may be one of the reasons for the reduced capacities of CO_2 absorption on Li_8ZrO_6 during the cycles but not the primary reason. Second, it is reported that the formed Li_2CO_3 molten phase could cause reconstruction and sintering of the lithium-based absorbent under high temperature and result in the gradual reduction of capacities during the cycles,[19] which may also be

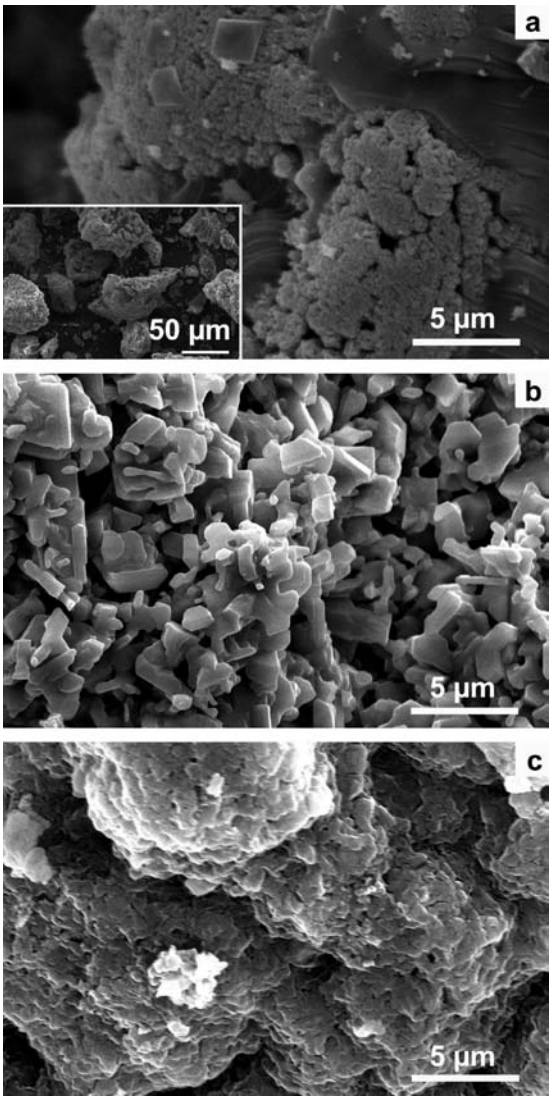

Figure 11. SEM images of the samples derived from Li_8ZrO_6 after CO_2 absorption and desorption. Image a corresponds to the CO_2 absorbed sample. Images b and c correspond to the samples that have undergone 1 and 11 cycles of CO_2 absorption−desorption, respectively.

available to explain the reduced capacity for Li_8ZrO_6. To validate this speculation, the samples that have undergone different absorption−desorption cycles are analyzed by SEM and BET, respectively. Figure 11 presents the SEM images of Li_8ZrO_6, including the CO_2-absorbed sample (corresponding to image a) and the regenerated samples (corresponding to images b and c). Compared with the images of the fresh sample in Figure 3a,b, the absorbed sample is comprised of larger particles with a loose layer covering the surface, which may be the carbonate layer formed as described in the other reports;[19,27] interestingly, the sample that has undergone one cycle of absorption−desorption is made up of large numbers of small particles with sizes of 1.0−3.0 μm (corresponding to image b), while the sample after 11 absorption−desorption cycles is seriously sintered (corresponding to image c). The results of BET analysis indicate that the surface areas of fresh Li_8ZrO_6 and the sample after one absorption−desorption cycle are decreased from 3.917 to 2.950 m^2 g^{-1} (24.7% reduction). These results confirm that reconstruction and sintering of the absorbent is serious under high temperature, subsequently

dx.doi.org/10.1021/ic102035y |*Inorg. Chem.* 2011, 50, 2844–2850

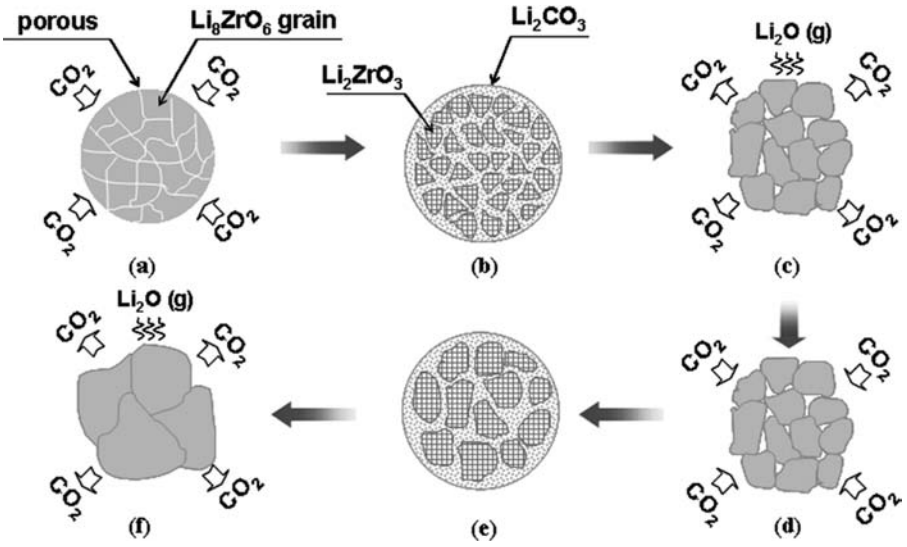

Figure 12. Schematic illustration for CO_2 absorption (at 1023 K) and desorption (at 1173 K) on Li_8ZrO_6. Steps a−c correspond to the first cycle of CO_2 absorption−desorption, and steps d−f correspond to the second cycle of CO_2 absorption−desorption.

causing the gradual reduction of capacities during the multicycle process.

On the basis of the above analysis, the multicycle process of CO_2 absorption−desorption can be depicted as steps a−f in Figure 12. At the initial step of CO_2 absorption, CO_2 may be easily diffused into the porosities of the Li_8ZrO_6 sample and quickly reacted with Li_8ZrO_6 to produce Li_2ZrO_3 and Li_2CO_3 (corresponding to step a); because of the expandability of the carbonate formed in the porosities, the large particles may be broken up as a mass of small particles surrounded with molten Li_2CO_3 combined with the loss of porosity (corresponding to step b); then the absorbed sample is desorbed in a N_2 flow, the Li_2ZrO_3 particles may react with the surrounded Li_2CO_3 to form reconstructed and sintered Li_8ZrO_6 particles, and the achieved particles are smaller compared with the initial large particles (corresponding to step c); besides, the surface area of the regenerated sample may also be reduced because of the loss of porosity, and fractional Li_2O may be sublimed as well. In the second cycle process of CO_2 absorption−desorption, the absorption rate may be slower than that at the initial step because of less surface area (corresponding to step e); moreover, the surface area of the absorbent may be further reduced, and the small particles may be sintered to larger particles in the regeneration process (corresponding to steps f and g); as a result, the rate of CO_2 absorption may be decreased, gradually combining with a reduced capacity for the following cycle.

CONCLUSIONS

High-purity Li_8ZrO_6 is successfully synthesized using $LiNO_3$ and $Zr(NO_3)_4$ by a three-step calcination method and characterized as a high-temperature CO_2 absorbent at different temperatures in varied CO_2 concentration atmospheres. The results indicate that the Li_8ZrO_6 produced possesses about 53.98 wt % capacity of CO_2 absorption above 998 K; moreover, almost 100% capacity could be preserved in a wide range of CO_2 concentrations (P_{CO_2} at 0.1−1.0 bar), which presents a great improvement in the scope of high-temperature CO_2 absorption on lithium-based ceramics. However, the capacity of CO_2 absorption on Li_8ZrO_6 is reduced gradually during the multicycle process mainly because of reconstruction and sintering of the absorbent under high temperature, which is the major limitation for utilization of Li_8ZrO_6 in high-temperature CO_2 capture from the flue gas of a coal-burning power plant and a SMR process.

ASSOCIATED CONTENT

Supporting Information. XRD analysis of the samples synthesized using LiOH and $Zr(NO_3)_4$ and percentages of different crystal phases in the products as a function of the initial Li/Zr molar ratios. This material is available free of charge via the Internet at http://pubs.acs.org.

AUTHOR INFORMATION

Corresponding Author

*E-mail: qhzhang@ecust.edu.cn. Tel/Fax: 86-21-64252171.

ACKNOWLEDGMENT

The research received financial support from National Science Foundation of China (20976047) and Special Nano Science and Technology Project of STCSM (0852 nm02100).

REFERENCES

(1) Ochoa-Fernández, E.; Rønning, M.; Grande, T.; Chen, D. *Chem. Mater.* **2006**, *18*, 1383–1385.
(2) Song, C. *Catal. Today* **2006**, *115*, 2–32.
(3) Ochoa-Fernández, E.; Haugen, G.; Zhao, T.; Rønning, M.; Aartun, I.; Børresen, B.; Rytter, E.; Rønnekleiv, M.; Chen, D. *Green Chem.* **2007**, *9*, 654–662.
(4) Ochoa-Fernández, E.; Rønning, M.; Grande, T.; Chen, D. *Chem. Mater.* **2006**, *18*, 6037–6046.
(5) Yi, K. B.; Eriksen, D. Ø. *Sep. Sci. Technol.* **2006**, *41*, 283–296.
(6) Xiong, R.; Ida, J.; Lin, Y. S. *Chem. Eng. Sci.* **2003**, *58*, 4377–4385.
(7) Ida, J.; Lin, Y. S. *Environ. Sci. Technol.* **2003**, *37*, 1999–2004.
(8) Choi, S.; Drese, J. H.; Jones, C. W. *ChemSusChem* **2009**, *2*, 796–854.
(9) Alcérreca-Corte, I.; Fregoso-Israel, E.; Pfeiffer, H. *J. Phys. Chem. C* **2008**, *112*, 6520–6525.

(10) Yong, Z.; Mata, V. G.; Rodrigues, A. E. *Ind. Eng. Chem. Res.* **2001**, *40*, 204–209.
(11) Xue, M.; Liu, Y.; Schaffino, R. M.; Xiang, S.; Zhao, X.; Zhu, G.-S.; Qiu, S.-L.; Chen, B. *Inorg. Chem.* **2009**, *48*, 4649–4651.
(12) Knofel, C.; Martin, C.; Hornebecq, V.; Llewellyn, P. L. *J. Phys. Chem. C* **2009**, *113*, 21726–21734.
(13) Thallapally, P. K.; Motkuri, R. K.; Fernandez, C. A.; McGrail, B. P.; Behrooz, G. S. *Inorg. Chem.* **2010**, *49*, 4909–4915.
(14) Nair, B. N.; Nakagawa, K.; Yanmaguchi, T. *Prog. Mater. Sci.* **2009**, *54*, 511–541.
(15) Nakagawa, K.; Ohashi, T. *J. Electrochem. Soc.* **1998**, *145*, 1344–1346.
(16) Essaki, K.; Kato, M. J. *J. Mater. Sci.* **2005**, *40*, 5017–5019.
(17) Rodríguez-Mosqueda, R.; Pfeiffer, H. *J. Phys. Chem. A* **2010**, *114*, 4535–4541.
(18) Pfeiffer, H.; Bosch, P. *Chem. Mater.* **2005**, *17*, 1704–1710.
(19) Yin, X.-S.; Song, M.; Zhang, Q.-H.; Yu, J.-G. *Ind. Eng. Chem. Res.* **2010**, *49*, 6593–6598.
(20) Ávalos-Rendón, T.; Casa-Madrid, J.; Pfeiffer, H. *J. Phys. Chem. A* **2009**, *113*, 6919–6923.
(21) Cruz, D.; Bulbulian, S.; Lima, E.; Pfeiffer, H. *J. Solid State Chem.* **2006**, *179*, 909–916.
(22) Wyers, G. P.; Cordfunke, E. *J. Nucl. Mater.* **1989**, *168*, 24–30.
(23) Zou, Y.; Petric, A. *J. Phys. Chem. Solids* **1994**, *55*, 493–499.
(24) Muhle, C.; Dinnebier, R. E.; Wullen, L. V.; Schwering, G.; Jansen, M. *Inorg. Chem.* **2004**, *43*, 874–881.
(25) Pfeiffer, H.; Bosch, P. *Mater. Chem. Phys.* **2002**, *78*, 558–561.
(26) Yin, X.-S.; Li, S.-P.; Zhang, Q.-H.; Yu, J.-G. *J. Am. Ceram. Soc.* **2010**, *93*, 2837–2842.
(27) Pannocchia, G.; Puccini, M.; Seggiani, M.; Vitolo, S. *Ind. Eng. Chem. Res.* **2007**, *46*, 6696–6706.